ACS APPLIED MATERIALS & INTERFACES

Research Article

www.acsami.org

Functionalized Graphene Sheets as a Versatile Replacement for Platinum in Dye-Sensitized Solar Cells

Joseph D. Roy-Mayhew,[†,‡] Gerrit Boschloo,[‡] Anders Hagfeldt,[‡] and Ilhan A. Aksay*[,†]

[†]Department of Chemical and Biological Engineering, Princeton University, Princeton, New Jersey 08544, United States

[‡]Department of Chemistry − Ångström Laboratory, Uppsala University, Box 523, 751 20 Uppsala, Sweden

Supporting Information

ABSTRACT: Several techniques for fabricating functionalized graphene sheet (FGS) electrodes were tested for catalytic performance in dye-sensitized solar cells (DSSCs). By using ethyl cellulose as a sacrificial binder, and partially thermolyzing it, we were able to create electrodes which exhibited lower effective charge transfer resistance (<1 Ω cm^2) than the thermally decomposed chloroplatinic acid electrodes traditionally used. This performance was achieved not only for the triiodide/iodide redox couple, but also for the two other major redox mediators used in DSSCs, based on cobalt and sulfur complexes, showing the versatility of the electrode. DSSCs using these FGS electrodes had efficiencies (η) equal to or higher than those using thermally decomposed chloroplatinic acid electrodes in each of the three major redox mediators: I (η_{FGS} = 6.8%, η_{Pt} = 6.8%), Co (4.5%, 4.4%), S (3.5%, 2.0%). Through an analysis of the thermolysis of the binder and composite material, we determined that the high surface area of an electrode, as determined by nitrogen adsorption, is consistent with but not sufficient for high performing electrodes. Two other important considerations are that (i) enough residue remains in the composite to maintain structural stability and prevent restacking of FGSs upon the introduction of the solvent, and (ii) this residue must not disperse in the electrolyte.

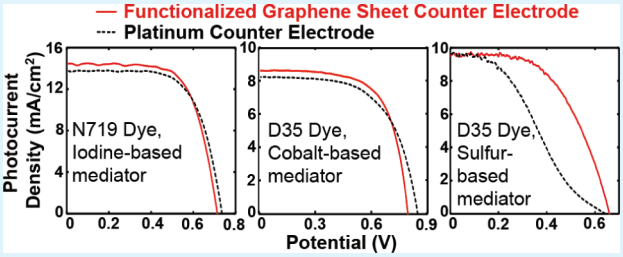

KEYWORDS: *graphene, dye-sensitized solar cell, cobalt redox mediator, triiodide, sacrificial binder*

1. INTRODUCTION

Dye-sensitized solar cells (DSSCs) are a potentially low cost alternative to silicon-based solar cells because of their easy fabrication and respectable energy conversion efficiency (over 10%).[1−3] The archetypical DSSC employs a porous film of sintered titania nanoparticles sensitized with an organometallic dye as a photoanode, a triiodide/iodide redox couple containing electrolyte, and a platinum coated transparent conductor (fluorine-doped tin oxide, FTO) catalytic cathode. In order to lower the cost and raise the efficiency of the device, prominent research efforts of the past twenty years have been on the optimization of DSSCs by developing dyes,[4] redox mediators,[5] and catalysts,[6] as well as improving the titania film morphology.[7] Because of slow interfacial charge recombination, triiodide/iodide mediated DSSCs have historically been the best performing devices. The redox potential of the triiodide/iodide redox couple (~0.35 V vs normal hydrogen electrode) is significantly more negative than that required for dye regeneration, limiting the open circuit voltage (V_{oc}) and hence power conversion efficiency (η) of the device.[8] Furthermore, the triiodide itself absorbs light, reducing the efficiency of the device. To overcome these limitations alternative redox couples have been explored[5] including cobalt-,[9] sulfur-,[10] and iron-based[11] compounds. Recently, Yella et al. have reported a new power conversion efficiency record of 12.3% for a DSSC using a zinc porphyrin dye, cosensitized with an organic dye, in conjunction with a cobalt-based redox mediator.[3]

A small loading of platinum nanoparticles (~5−10 μg/cm^2), created through the thermal decomposition of chloroplatinic acid, has been the dominant counter electrode catalyst material since its introduction in 1997.[6,12] While platinum is very effective for catalyzing the reduction of triiodide, it is less effective as a catalyst in the cobalt redox system, and particularly poor with sulfur-based mediators.[10,13] Concerns over platinum's cost and stability have led to a plethora of studies, primarily with the iodine-based mediator, examining alternative catalysts such as CoS,[14] polymers,[15] and carbon nanomaterials including carbon black,[16,17] carbon nanotubes,[18,19] and reduced graphene oxide.[20−22] Yet, to date, there have been no reports of an alternative catalyst to platinum that can match − or exceed − this precious metal's performance with multiple redox couples.

To replace platinum on a DSSC cathode with a less expensive catalyst, previously we reported on porous networks of functionalized graphene sheets (FGSs) created by the thermolysis of a binder in an FGS-polymer composite.[20] DSSCs using FGS networks performed 90% as well as cells using

Received: March 13, 2012
Accepted: May 1, 2012
Published: May 1, 2012

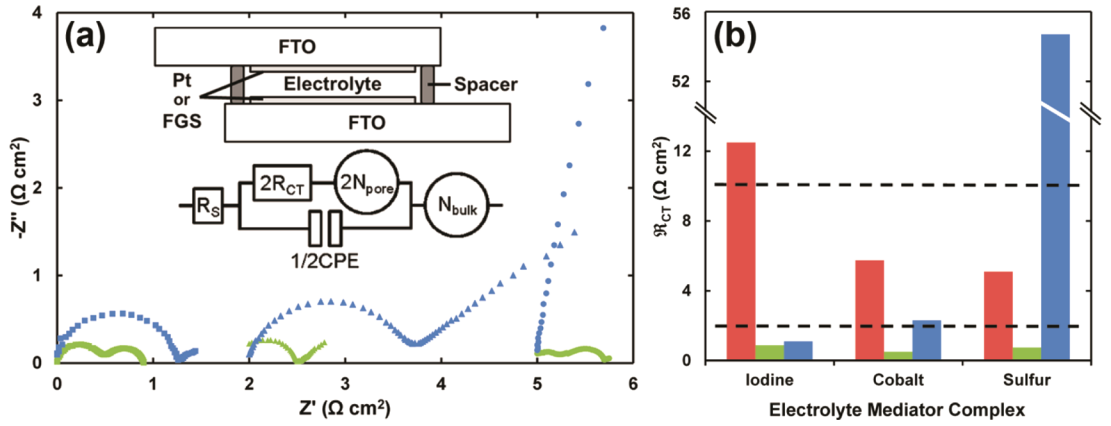

Figure 1. Comparison of $\mathscr{R}_{CT}$ for counter electrodes using acetonitrile electrolyte with I-, Co-, and S-based mediators. (a) Impedance spectra of FGS (green) and Pt (blue) electrodes. Squares: I-based mediator; Triangles: Co-based mediator; Circles: S-based mediator. Spectra were shifted on the *x*-axis for easier comparison. Upper inset: Sandwich cell setup to test counter electrode performance. Lower inset: Equivalent circuit for this setup. R_S: series resistance; R_{CT}: charge-transfer resistance of one electrode; CPE: constant phase element of one electrode; N_{pore}: Nernst diffusion impedance within electrode pores; N_{bulk}: Nernst diffusion impedance between the electrodes. (b) Summary of effective charge transfer resistance ($\mathscr{R}_{CT} = R_{CT} + N_{pore}$) of electrodes. Red: FGS counter electrodes using the formulation from our previous work.[20] Green: FGS counter electrodes described in this work. Blue: Thermally decomposed chloroplatinic acid electrodes. Dotted lines represent common counter electrode targets, upper: 10 Ω cm^2 from Hauch and Georg,[32] lower: 2 Ω cm^2 from Trancik et al.[19] $\mathscr{R}_{CT}$ was determined using EIS using a sandwich cell configuration. See Supporting Information for more information.

platinum as a catalyst. FGSs are a type of defective graphene currently synthesized at the industrial scale[23] via the simultaneous thermal exfoliation and reduction of graphite oxide (GO), detailed elsewhere.[24,25] FGSs have a large surface area (up to 1850 m^2/g as measured in a colloidal state) and contain lattice defects and oxygen-containing functional groups, such as hydroxyls, epoxides, and carboxylic acids, making it a promising material for catalysis.[24,26,27] Similar results using other graphene-based materials were later reported using different processing techniques such as drop casting,[28] electrophoretic deposition,[29] and screen printing.[21] Recently, Kavan et al. showed that graphene nanoplatelet (1−15 nm thick stacks of graphene) coated electrodes could outperform platinum for the reduction of the cobalt mediator; however, these electrodes did not perform as well as platinum in the iodine-based system.[28,30,31]

Herein, we describe a new FGS-sacrificial binder system, using ethyl cellulose, in which the thermolysis of the binder increases the FGS surface area available for catalysis while the binder residue improves the electrode's structural stability in acetonitrile-containing electrolytes. This process yields versatile electrodes that perform as well as or better than platinum in I-, Co-, and S-based redox systems. Furthermore, we analyze how processing conditions affect electrode performance and suggest system characteristics required for high performing electrodes. Although the resultant FGS film is not transparent, the FGS paste requires only a single doctor blade layer and can directly replace current platinum pastes used in DSSC manufacturing.

2. RESULTS AND DISCUSSION

2.1. Counter Electrode Performance. We evaluate the performance of counter electrodes by directly measuring their catalytic activity and then support these results by characterizing DSSCs which use the electrodes. The catalytic performance of a DSSC cathode is quantified by the charge transfer resistance (R_{CT}) of the electrolyte-cathode interface. Two commonly referenced performance targets for the DSSC cathode R_{CT} are less than 10 Ω cm^2,[32] and 2−3 Ω cm^2.[19] Electrochemical Impedance Spectroscopy (EIS), with an appropriate equivalent circuit, is used to determine the R_{CT} for the reduction of triiodide on platinum electrodes at electrolyte concentrations used in DSSCs.[12,32] We recently expanded this equivalent circuit to be applicable to highly porous electrodes (for details, refer to the Supporting Information).[20] Characteristic impedance spectra taken at 0 V bias are presented in Figure 1a. The inserts of Figure 1a show the sandwich cell configuration used for testing and the EIS equivalent circuit. Following the IUPAC convention, Z' and Z'' are the real and imaginary parts of the impedance, respectively.[33] These spectra have been normalized to the geometric surface area of the catalyst on an electrode. For the experimental setup used, series resistance (R_s) was about 12 Ω for both FGS- and platinum-based electrodes. Scaling by area holds little meaning for R_s, and, thus, the spectra have been shifted to clearly compare FGS and platinum-based electrodes for the I-, Co-, and S-based electrolyte systems. The parameter of interest in this system is the combined contribution of the catalytic R_{CT} and transport impedance in the pores, modeled by a Nernst diffusion element (N_{pores}). We term this sum the effective charge transfer resistance, $\mathscr{R}_{CT,}$ where $\mathscr{R}_{CT} = R_{CT} + N_{pores}$. For nonporous electrodes, such as the thermally decomposed platinic acid electrodes used in this study, N_{pores} can be neglected and $R_{CT} = \mathscr{R}_{CT}$. For highly catalytic FGS electrodes, transport resistance in the pores represents a significant component of $\mathscr{R}_{CT}$ and thus cannot be neglected.

Impedance results are summarized in Figure 1b, which also includes electrodes made from the method in our earlier work.[20] As can be seen, not only have the $\mathscr{R}_{CT}$ values of our electrodes decreased by an order of magnitude, but they meet the more stringent performance standard as well, and they are lower than those obtained using thermally decomposed chloroplatinic acid. Moreover, unlike platinum, FGSs perform well as a catalyst in all three electrolyte systems tested, showing their versatility.

To ensure that the new FGS electrodes are indeed superior to platinized FTO when incorporated into a device, we compare current density−voltage curves of DSSCs using the

two types of counter electrodes (Figure 2). Average V_{oc}, short circuit current density (J_{sc}), fill factor (FF), and η for devices

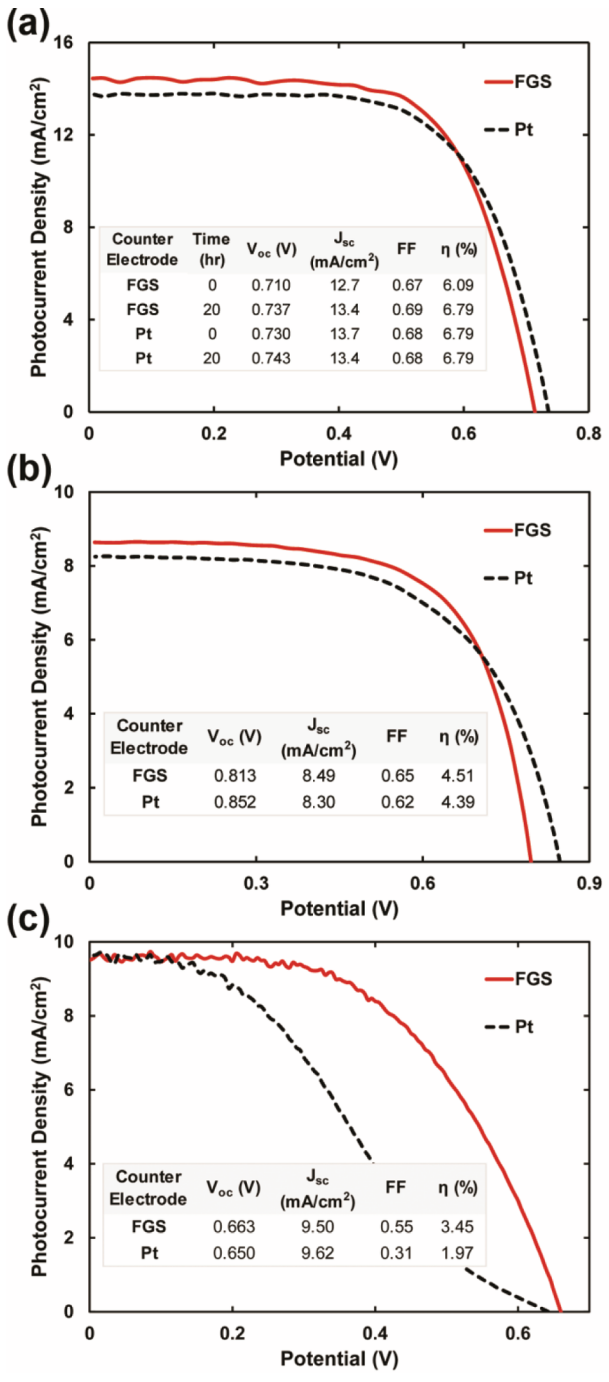

Figure 2. $J-V$ curve characteristics of DSSCs using thermally decomposed chloroplatinic acid (Pt) and FGS counter electrodes. (a) I-based mediator, N719 sensitizer; (b) Co-based mediator, D35 sensitizer; (c) S-based mediator, D35 sensitizer. Active area is 0.25 cm^2.

tested are tabulated in the inserts. Herein, η is defined as the cell's maximum power output (P_{max}) divided by the input power from the light source and $FF = P_{max}/(I_{sc}V_{oc})$, where I_{sc} is the short circuit current of the cell. For all three electrolyte systems tested, DSSCs using FGS cathodes perform as well as or better than those using platinized FTO cathodes, in agreement with our EIS results. Furthermore, across all electrolytes, the FF of the devices using FGS is higher than that of those using platinum. This result is consistent with a lower $\mathscr{R}_{CT}$ for these devices that we see with the EIS data. We note that for a few samples, DSSCs using FGS electrodes performed significantly worse than the rest of the data set; thus, to prevent skewing of our data with outliers, we did not include these results in our average tabulation. The results presented are indicative of what we can achieve, and although we are not sure why a minority of cells behaved poorly, it could be due to variations in the processing of the film. After doctor-blading, when the tape mask is removed, part of the edge of the FGS film may also lift up resulting in a short circuit from the counter electrode to the photoanode. If so, fabricating electrodes through tape casting or screen printing would eliminate this issue.

Interestingly, for DSSCs using an iodine-based electrolyte (Figure 2a), solar cell performance improved markedly over the first day. Components of the electrolyte such as 4-tert-butylpyridine (TBP) and iodine may be adsorbing to the porous electrodes during this time.[34] Although it is out of the scope of this work, we are currently examining the potential role of iodine adsorption. An alternative explanation is that it may take time for the electrolyte to fully infiltrate the FGS film. Thus, over time, more surface area would be accessible to catalyze the reduction of triiodide. However, sandwich cell electrodes show strong catalytic activity shortly after fabrication, and $\mathscr{R}_{CT}$ actually increases slightly (by ~10%) after a day, negating this conjecture.

The DSSCs presented in Figure 2b use similar materials to those used in the landmark paper by Feldt et al. on codesigning the dye and cobalt redox couple.[9] As fast recombination between the conduction band of TiO_2 and cobalt mediators has limited DSSC performance for devices using traditional dyes such as N719, in this study a dye with bulky side chains (D35) is used. Butoxyl chains on D35 sterically hinder the interaction of cobalt complexes with TiO_2, reducing recombination in the device. The lower performance exhibited in the current work compared to that of Feldt et al. is likely due to the use of TiO_2 with a smaller primary particle size in the DSL18-NR-T paste (the DSL30 NRD-T paste used by Feldt et al. has been discontinued). This explanation is consistent with the finding by Yella et al. that smaller pores impede the transport of the relatively large cobalt complexes and decrease device efficiency.[3] Although FF is higher for the cell with the FGS cathode as expected due to the lower $\mathscr{R}_{CT}$, the V_{oc} is lower. This observation is also made in two works by Kavan et al. and they explain that it could be due to a higher dark current in the devices using graphene nanoplatelet electrodes.[30,31] Graphene nanoplatelets detaching from the FTO electrode and depositing on the TiO_2 film, a concern with other carbon electrodes, could explain this observation.[16,35,36] An alternative explanation is that the electrolyte can infiltrate the whole FGS film including pores which are too small for the cobalt redox couple to access. This would shift the electrolyte concentration in the active part of the solar cell and could influence the electrolyte redox potential, and thus V_{oc} of the device.

The effect of platinum's high $\mathscr{R}_{CT}$ on the FF of devices with the sulfur-based mediator is clearly seen in Figure 2c. The lower V_{oc} compared to the cobalt-based device is due to the more negative potential of the electrolyte. The greater J_{sc} is due, at least in part, to the lower light absorption by the sulfur based mediator. The FGS electrodes in these devices were only

heated to 310 °C, and even though the $\mathscr{R}_{CT}$ is low (0.75 Ω cm^2) it is likely not optimal.

2.2. Counter Electrode Processing. The high performing FGS electrodes presented above were created by first doctor blading an FGS-ethyl cellulose paste onto FTO and then partially thermolyzing the binder in air. In order to understand why FGS electrodes using ethyl cellulose as a sacrificial binder performed better than those fabricated using other binders and methods, we examined the effect of electrode processing (for EIS data on other processing routes, see the Supporting Information, Figure S1). We first look at how processing affects the catalytic performance of the electrode, and then relate this to the respective changes in residue amount and electrode surface area.

As seen in Table 1, $\mathscr{R}_{CT}$ is highly dependent on the heat treatment process for removing the binder. $\mathscr{R}_{CT}$ decreases as temperature is increased up until heat treatments at 370 °C, above which $\mathscr{R}_{CT}$ increases. Nevertheless, as seen in Table 1, heating anywhere from 330 to 420 °C and holding for 12 min resulted in electrodes with $\mathscr{R}_{CT}$ below 3 Ω cm^2 with the iodine-based redox system.

Table 1. Effect of Heat Treatment on Counter Electrode Performance[a]

T (°C)	N_{pore} (Ω cm^2)	R_{CT} (Ω cm^2)	$\mathscr{R}_{CT}$ (Ω cm^2)
25		84.5	84.5
270	3.4	5.5	8.8
300	1.7	15.1	16.8
330	0.4	2.0	2.4
350	0.5	1.2	1.8
370	0.5	0.4	0.9
420	0.6	1.3	2.0
450	0.7	5.5	6.1

[a]Heat treatment is under air holding at the prescribed temperature for 12 min.

During heat treatment, the ethyl cellulose binder melts and decomposes as shown in Figure 3. Higher temperature heat treatments result in more of the ethyl cellulose being removed. About 6, 12, and 42% of the binder is removed during heat treatments at 270, 300, and 330 °C, respectively. These values were affirmed not only by thermogravimetric analysis (TGA), but also by heating 1 g of ethyl cellulose with the samples and massing the residue. Heat treatment has a small effect on the FGSs as well. FGSs are stable until about 420 °C, but a 4% mass loss occurs upon treatment to 450 °C, the highest temperature examined in this study (see Figure S2 in the Supporting Information).

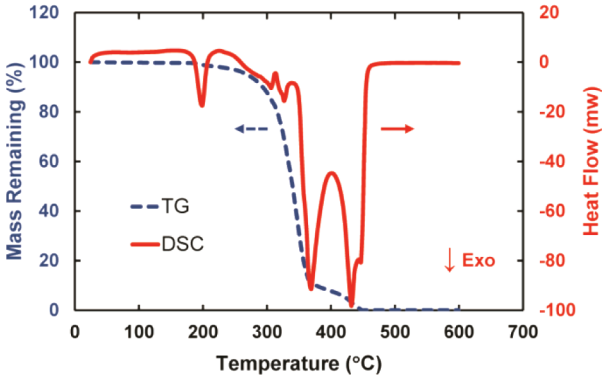

Figure 3. Simultaneous thermal analysis of ethyl cellulose thermolysis in air. Blue dotted line: thermal gravimetric analysis. Red line: differential scanning calorimetry, where negative heat flow represents an exothermic event.

As seen in Table 2, electrode surface area increases monotonically as ethyl cellulose is removed, while the surface area of FGSs in the electrodes reaches a maximum at a heat treatment of 330 °C. The specific surface area of FGSs in a heat treated electrode is approximated (eq 1) by taking the surface area of the composite electrode after heat treatment, and subtracting out that portion which can be attributed to the ethyl cellulose residue

$$SA_{FGS} = \frac{(m_{FGS} + m_{ECRes})SA_{Comp} - m_{ECRes}SA_{ECRes}}{m_{FGS}} \quad (1)$$

where SA_{FGS} is the calculated specific surface area of FGS in the composite, SA_{Comp} is the measured composite specific surface area, SA_{ECRes} is the measured ethyl cellulose residue specific surface area, m_{FGS} is the mass of FGS in the composite, and m_{ECRes} is the mass of ethyl cellulose in the composite.

With low-temperature heat treatments (270 °C), ethyl cellulose has a residue with a dense, glasslike structure. The residue's surface area is very low (<1 m^2/g) and its mass percentage of the electrode is high (~65 wt %). At high temperatures (450 °C), the specific surface area of the ethyl cellulose residue is high (237 m^2/g), however, its mass percentage of the electrode is low (~3.8 wt %). Thus, although the specific surface area of the composite increases with heat treatment intensity, the specific surface area for FGSs can be higher at lower heat treatments.

A main distinction from our previous work[20] is that for our best performing electrodes a significant amount of binder residue (~20 wt % of the electrode) remains after heat treatment. A similar optimum was recently found by Zhang et al., who attributed their results to a decrease in, but not complete removal of, the electrode binder.[21] More specifically, we maintain that the high performance of our 370 °C heat-treated electrodes is due to the residue acting as a stable spacer for FGSs, as evidenced by the residue's insolubility in the electrolyte and the high surface area of the catalytically active FGSs after drying.

To explain this effect with more certainty, we look at the role of ethyl cellulose in the electrodes. Ethyl cellulose is used as both a dispersant and a binder for casting the electrode film. Drying FGS suspensions without the binder causes FGSs to stack into structures with lower specific surface areas. With a binder, a composite is formed in which the binder is present between sheets, keeping them separated during solvent evaporation.[37] The removal of the binder from the composite opens up the space between the sheets and increases the surface area of the electrode.[37] Because the catalytic activity of the electrode should be proportional to the surface area, we expect a higher surface area to correspond to a lower R_{CT}. As evidenced by the decreasing resistance to transport (N_{pore}) with increasing heat treatment, the pores are more accessible as binder is removed; however, the electrode surface area correlates with catalytic performance only up to heat treatments of 370 °C, after which $\mathscr{R}_{CT}$ increases.

Although it is clear that binder blocking active sites and inhibiting diffusion can reduce the effective catalytic activity, it is less obvious why electrode performance decreases upon

Table 2. Characteristics of Ethyl Cellulose and Composites of FGS and Ethyl Cellulose after Heat Treatments at Various Temperatures

	polymer (ethyl cellulose)			composite (FGS and ethyl cellulose)			
T (°C)	residue fraction	solubility of residue in acetonitrile	residue surface area (m^2/g)	surface area (m^2/g)	calcd FGS surface area (m^2/g)	surface area (m^2/g) after acetonitrile wash	calcd FGS surface area (m^2/g) after acetonitrile wash
25	1.00	soluble	<1	37	109		
270	0.94	soluble	<1	74	212		
300	0.87	soluble	<1	155	424		
330	0.58	soluble	<1	296	637		
350	0.19	partially soluble	3	348	480	349	480
370	0.13	insoluble	28	392	451	383	475
420	0.06	insoluble	210	455	483	391	412
450	0.02	insoluble	237	479	489	386	392

removing more than 90% of the binder. In short, why does having some binder residue improve performance? Two possible explanations are that the residue itself is catalytic to the reaction, or the residue is improving the catalytic activity of the electrodes by improving the FGS accessible surface area, perhaps by acting as pillars separating sheets. EIS analysis of sandwich cells made with ethyl cellulose residue shows no measurable catalytic activity toward the reduction of triiodide, discounting this possibility. When only accounting for the surface area of the FGS in the electrodes, which is consistent with it being the catalytically active material, we see higher surface areas at lower temperature heat treatments, supporting the conjecture that the binder aids in keeping the sheets apart. Nevertheless, the lowest R_{CT} is seen with heat treatment at 370 °C and not at 330 °C − the temperature which results in the largest FGS surface area − so another factor must play a role. One possibility is that the characteristics of the electrode examined in air are not the best representation of the material in a device, for our case, in acetonitrile.

As we cannot examine the electrodes in situ, we used two proxies to provide a qualitative assessment of electrode stability in the electrolyte. First, we looked at whether the residual binder was soluble in acetonitrile (see Table 2 for summary, Figure S3 in the Supporting Information for images). Ethyl cellulose swells but is not soluble in acetonitrile. However, upon minor heat treatment, the residue is readily soluble. Between 330 and 350 °C, a transition occurs in which some of the residue is carbonized enough to be insoluble in the electrolyte and by 370 °C, the residue is completely insoluble. Thus, although electrodes heat-treated below 330 °C may have a higher FGS surface area in air, upon exposure to the electrolyte, the binder will dissolve. Without adequate spacers, FGSs could then restack, reducing the surface area available for catalysis.

For a second proxy, we looked at the surface area of the electrodes after they had been soaked in acetonitrile and dried (Table 2). Although drying is not expected to occur in actual devices, this experiment can provide insight into the stability of the electrodes. Only electrodes that had residues insoluble to acetonitrile were tested in this way. Electrodes heat-treated to 350 and 370 °C had about the same surface area before and after the wash, which shows that the electrode structure is relatively stable. X-ray diffraction (XRD) also shows no significant change in the intensity or d-spacing of the samples (see Figure S4 in the Supporting Information). On the other hand, electrodes heated to 420 and 450 °C experienced a significant decline in surface area. In these two cases, only a small amount of ethyl cellulose is present. This residue may be insufficient to keep FGSs apart upon stressing the system, such as the introducing an electrolyte solution. For the 450 °C case, the XRD pattern did shift after drying showing that the structure is not stable (see Figure S4 in the Supporting Information). Interestingly, the intensity decreased after drying and it appears as though there is a smaller signal at ∼26.4°, characteristic (0002) graphite spacing. In our previous study,[37] the binder was almost completely removed from the electrodes; thus, as with the case of high temperature heat treatments with FGS:ethyl cellulose electrodes, there may have been a lack of adequate residue for stability which could explain their relatively poor performance.

From the above analysis we present the following as important considerations for an FGS composite counter electrode: (i) the FGS in the heat treated composite material (FGS:ethyl cellulose residue) must have high surface area; (ii) the binder residue must be insoluble in the electrolyte (in this case, acetonitrile); and (iii) enough residue must remain in the composite to retain stability of the FGS network upon the introduction of solvent.

3. CONCLUSION

By using ethyl cellulose as a sacrificial binder, and partially thermolyzing it, we created versatile functionalized graphene sheet (FGS) counter electrodes for Dye-Sensitized Solar Cells (DSSCs). These electrodes exhibited lower effective charge transfer resistance than that of the thermally decomposed platinic acid electrodes for DSSCs with I-, Co-, and S-based redox mediators. With each of these redox mediators, DSSC using FGS counter electrodes had efficiencies equal to or higher than those using the platinic acid-derived electrodes. Through analyzing FGS electrode processing conditions, we found that surface area and stability are important considerations for high performance. In particular, enough binder residue should remain in the composite to maintain structural stability and prevent restacking of FGSs upon the introduction of the solvent, and this residue should not disperse in the electrolyte. Although the resulting films are not highly transparent, FGS:ethyl cellulose pastes provide an effective replacement to platinum pastes currently used in the manufacture of DSSCs, and have the added benefit of working better with a wide range of redox mediators.

4. EXPERIMENTAL SECTION

Preparation of Counter Electrodes. FGS counter electrodes were prepared on FTO (TEC8, Hartford Glass). Pastes (described below) were tip sonicated for 30 s before use and then doctor bladed on a tape spacer resulting in ∼6 μm thick films after drying at room

temperature. Electrodes then underwent heat treatment under air in an oven (Nabertherm Controller P320).

FGS:Ethyl Cellulose Electrodes. 0.3 g of FGS (Vor-x batch BK86x, Vorbeck Materials Inc.) was added to 6 g of 10 wt % ethyl cellulose in ethanol. To achieve desired thickness of the films after drying, 11 g of ethanol was added. This mixture was then mixed and tip sonicated at 40% power (Vibra-Cell VCX 750) for 2 min. Heat treatment of films was performed in air at a range of temperatures from 270 to 450 °C for 12 min, ramping at 10 °C/min.

Original FGS Electrodes. FGS-surfactant (poly(ethylene oxide)-poly(propylene oxide)-poly(ethylene oxide) triblock copolymer, F127, Pluronic) suspension (1.66 wt % FGS, 1.66 wt % surfactant in water) was mixed in a poly(ethylene oxide) (PEO, M_v 600 000) solution (0.6 g in 10 mL water, 10 mL ethanol) in a 1:4 FGS:PEO mass ratio and stirred overnight.[20] Electrodes were heat treated at 350 °C for 2 h.

Platinized Electrodes. A 4.8 mM chloroplatinic acid solution in ethanol was deposited onto the FTO glass substrate (10 μL/cm^2) and heated to 400 °C for 30 min before use.

Preparation of DSSCs. DSSCs were constructed as described previously in the literature.[9] In brief, FTO glass (TEC15, Hartford Glass) was cleaned in an ultrasonic bath overnight in ethanol. A TiO_2 underlayer was formed by pretreating the glass at 70 °C in 40 mM $TiCl_4$ solution for 30 min. The films were then subsequently washed with water and ethanol. TiO_2 films, 0.5 × 0.5 cm^2, were prepared by screen printing 2 layers of a colloidal TiO_2 paste (Dyesol DSL 18 NR-T). Two layers of a scattering layer (PST-400C, received from JGS Catalysts and Chemicals) was then screen printed on top of the TiO_2 nanoparticle film. Resulting films had a thickness of ∼18 μm. The electrodes were heated (Nabertherm Controller P320) in an air atmosphere at 180 °C (10 min), 320 °C (10 min), 390 °C (10 min), and 500 °C (30 min). A final $TiCl_4$ treatment was performed similar to above, and the electrodes were sintered again using the above protocol. Before use, electrodes were heated to 300 °C to remove water, and allowed to cool to 80 °C before being placed in a dye solution overnight. The films were then rinsed using the same solvent and dried. Platinum and FGS counter electrodes were formed as described above. A 50 μm Surlyn thermoplastic film was used to separate the photoanode and the counter electrode and to seal the cell after electrolyte was added.

A 0.3 mM N719 dye solution in 1:1 acetonitrile:tert-butanol was used for DSSCs with the iodine-based electrolyte (0.6 M tetrabutylammonium iodide, 0.1 M lithium iodide, 0.05 M iodine, 0.2 M 4-tert-butylpyridine in acetonitrile). A 0.2 mM D35 dye solution in ethanol was used for DSSCs with the cobalt- (0.22 M $Co(bpy)_3(PF_6)_2$, 0.033 M $Co(bpy)_3(PF_6)_2$ where bpy = 2,2′-bipyridine, 0.1 M lithium perchlorate, 0.2 M 4-tert-butylpyridine in acetonitrile) and sulfur- (0.1 mM dimethyldithiocarbamate (M-) 0.1 M 5-mercapto-1-methyltetrazole dimer (T_2), 0.5 M 4-tert-butylpyridine in acetonitrile)-based electrolytes.

Measurements. EIS was performed using a Biologic SP-150 potentiostat and a CH Instruments 760C potentiostat using a sandwich cell configuration (50 μm spacing) in which symmetric electrodes were infiltrated with the same electrolyte as used in the DSSCs. EIS measurements were taken at 0 V, the magnitude of the alternating signal was 10 mV, and the frequency range was 1 Hz to 100 kHz. ZFit (Biologic), with the appropriate equivalent circuit, was used to analyze the impedance spectra. Current−voltage characteristics of DSSCs were taken under AM1.5G light, simulated at 1000 W/m^2 using two setups: (i) a 16S solar simulator (SolarLight) calibrated with PMA2144 pyranometer (SolarLight) using the Biologic potentiostat and (ii) a Newport solar simulator (model 91160) calibrated with a certified reference cell (Fraunhofer ISE) using a Keithley 2400 source/meter. Data values presented are the average of 2−6 identically prepared samples, while figures are representative of individual runs.

Ethyl cellulose decomposition was examined by simultaneous thermal analysis (STA; 449 C Jupiter, Erich Netzsch GmbH & Co.) incorporating a thermogravimetric analyzer and a differential scanning calorimeter (DSC). Platinum pans were used and all STA measurements were done under flowing air (40 mL/min) at a ramp rate of 10 K/min. The DSC was calibrated using a set of standards (In, Sn, Bi, Zn, CsCl) with well-known temperatures and enthalpies of phase transitions.

Electrode surface area was determined from nitrogen adsorption by the Brunauer, Emmett, and Teller (BET) method[38] using a surface area analyzer (Gemini V, Micromeritics Instrument Corporation). Samples were dried for 3 h at 160 °C under vacuum before measurement.

To analyze the degree of FGS stacking in samples, we obtained X-ray diffraction (XRD) patterns using a desktop diffractometer (Rigaku MiniFlex II, Cu K_α radiation at λ = 1.54 Å) sampling at 2°/min, 30 kV and 15 mA.

■ ASSOCIATED CONTENT

Ⓢ Supporting Information

Impedance data on alternative electrode processing routes (Figure S1); simultaneous thermal analysis of FGS (Figure S2); images of ethyl cellulose residue dispersion (Figure S3); X-ray diffraction patterns of heat treated electrodes, pre- and postwash (Figure S4). This material is available free of charge via the Internet at http://pubs.acs.org

■ AUTHOR INFORMATION

Corresponding Author

*E-mail: iaksay@princeton.edu.

Notes

The authors declare no competing financial interest.

■ ACKNOWLEDGMENTS

The authors thank P. Lohse (Uppsala University) for supplying the cobalt redox mediator, C. Woohyung (Hanyang University) for supplying the sulfur mediator, J. S. Lettow (Vorbeck Materials Corporation) for supplying Vor-x, and K. Nonomura (Uppsala University) for his kind assistance. J.D.R.-M. was supported by the National Science Foundation Graduate Research Fellowship under Grant DGE-0646086. This work was supported by the Pacific Northwest National Laboratory (operated for the United States Department of Energy by Battelle) through Battelle Grant 66354 and the Army Research Office (ARO)/Multidisciplinary Research Initiative (MURI) under Grant W911NF-09-1-0476.

■ REFERENCES

(1) O'Regan, B.; Grätzel, M. *Nature* **1991**, *353*, 737−740.
(2) Grätzel, M. *Inorg. Chem.* **2005**, *44*, 6841−6851.
(3) Yella, A.; Lee, H.-W.; Tsao, H. N.; Yi, C.; Chandiran, A. K.; Nazeeruddin, M. K.; Diau, E. W.-G.; Yeh, C.-Y.; Zakeeruddin, S. M.; Grätzel, M. *Science* **2011**, *334*, 629−634.
(4) Hagfeldt, A.; Boschloo, G.; Sun, L.; Kloo, L.; Pettersson, H. *Chem. Rev.* **2010**, *110*, 6595−6663.
(5) Tian, H.; Sun, L. *J. Mater. Chem.* **2011**, *21*, 10592−10601.
(6) Murakami, T. N.; Grätzel, M. *Inorg. Chim. Acta* **2008**, *361*, 572−580.
(7) Zhang, Q.; Cao, G. *Nano Today* **2011**, *6*, 91−109.
(8) Boschloo, G.; Hagfeldt, A. *Acc. Chem. Res.* **2009**, *42*, 1819−1826.
(9) Feldt, S. M.; Gibson, E. A.; Gabrielsson, E.; Sun, L.; Boschloo, G.; Hagfeldt, A. *J. Am. Chem. Soc.* **2010**, *132*, 16714−16724.
(10) Wang, M.; Chamberland, N.; Breau, L.; Moser, J.-E.; Humphry-Baker, R.; Marsan, B.; Zakeeruddin, S. M.; Grätzel, M. *Nat. Chem.* **2010**, *2*, 385−389.
(11) Daeneke, T.; Kwon, T.-H.; Holmes, A. B.; Duffy, N. W.; Bach, U.; Spiccia, L. *Nat. Chem.* **2011**, *3*, 211−215.
(12) Papageorgiou, N.; Maier, W. F.; Grätzel, M. *J. Electrochem. Soc.* **1997**, *144*, 876−884.
(13) Tian, H.; Yu, Z.; Hagfeldt, A.; Kloo, L.; Sun, L. *J. Am. Chem. Soc.* **2011**, *133*, 9413−9422.

(14) Wang, M.; Anghel, A. M.; Marsan, B.; Cevey, Ha, N.-L.; Pootrakulchote, N.; Zakeeruddin, S. M.; Grätzel, M. *J. Am. Chem. Soc.* **2009**, *131*, 15976−15977.
(15) Ahmad, S.; Yum, J.-H.; Butt, H.-J.; Nazeeruddin, M. K.; Grätzel, M. *ChemPhysChem* **2010**, *11*, 2814−2819.
(16) Kay, A.; Grätzel, M. *Sol. Energy Mater. Sol. Cells* **1996**, *44*, 99−117.
(17) Murakami, T. N.; Ito, S.; Wang, Q.; Nazeeruddin, M. K.; Bessho, T.; Cesar, I.; Liska, P.; Humphry-Baker, R.; Comte, P.; Pechy, P.; Grätzel, M. *J. Electrochem. Soc.* **2006**, *153*, A2255−A2261.
(18) Nam, J. G.; Park, Y. J.; Kim, B. S.; Lee, J. S. *Scr. Mater.* **2010**, *62*, 148−150.
(19) Trancik, J. E.; Barton, S. C.; Hone, J. *Nano Lett.* **2008**, *8*, 982−987.
(20) Roy-Mayhew, J. D.; Bozym, D. J.; Punckt, C.; Aksay, I. A. *ACS Nano* **2010**, *4*, 6203−6211.
(21) Zhang, D. W.; Li, X. D.; Li, H. B.; Chen, S.; Sun, Z.; Yin, X. J.; Huang, S. M. *Carbon* **2011**, *49*, 5382−5388.
(22) Hasin, P.; Alpuche-Aviles, M. A.; Wu, Y. *J. Phys. Chem. C* **2010**, *114*, 15857−15861.
(23) Vorbeck Materials Corporation: Jessup, MD.
(24) Schniepp, H. C.; Li, J.-L.; McAllister, M. J.; Sai, H.; Herrera-Alonso, M.; Adamson, D. H.; Prud'homme, R. K.; Car, R.; Saville, D. A.; Aksay, I. A. *J. Phys. Chem. B* **2006**, *110*, 8535−8539.
(25) McAllister, M. J.; Li, J.-L.; Adamson, D. H.; Schniepp, H. C.; Abdala, A. A.; Liu, J.; Herrera-Alonso, M.; Milius, D. L.; Car, R.; Prud'homme, R. K.; Aksay, I. A. *Chem. Mater.* **2007**, *19*, 4396−4404.
(26) Kudin, K. N.; Ozbas, B.; Schniepp, H. C.; Prud'homme, R. K.; Aksay, I. A.; Car, R. *Nano Lett.* **2007**, *8*, 36−41.
(27) Schniepp, H. C.; Kudin, K. N.; Li, J.-L.; Prud'homme, R. K.; Car, R.; Saville, D. A.; Aksay, I. A. *ACS Nano* **2008**, *2*, 2577−2584.
(28) Kavan, L.; Yum, J. H.; Grätzel, M. *ACS Nano* **2010**, *5*, 165−172.
(29) Choi, H.; Kim, H.; Hwang, S.; Han, Y.; Jeon, M. *J. Mater. Chem.* **2011**, *21*, 7548−7551.
(30) Kavan, L.; Yum, J.-H.; Nazeeruddin, M. K.; Grätzel, M. *ACS Nano* **2011**, *5*, 9171−9178.
(31) Kavan, L.; Yum, J.-H.; Grätzel, M. *Nano Lett.* **2011**, *11*, 5501−5506.
(32) Hauch, A.; Georg, A. *Electrochim. Acta* **2001**, *46*, 3457−3466.
(33) *IUPAC Compendium of Chemical Terminology*, 2nd ed.; Compiled by McNaught, A. D., Wilkinson., A. Blackwell Scientific Publications, Oxford, U.K., 1997. XML on-line corrected version: http://goldbook.iupac.org (2006) created by Nic, M.; Jirat, J.; B. Kosata; updates compiled by Jenkins, A..
(34) Hu, H.; Chen, B.-L.; Bu, C.-H.; Tai, Q.-D.; Guo, F.; Xu, S.; Xu, J.-H.; Zhao, X.-Z. *Electrochimic. Acta* **2011**, *56*, 8463−8466.
(35) Lee, W. J.; Ramasamy, E.; Lee, D. Y.; Song, J. S. *ACS Appl. Mater. Interfaces* **2009**, *1*, 1145−1149.
(36) Lee, W. J.; Ramasamy, E.; Lee, D. Y.; Song, J. S. *Sol. Energy Mater. Sol. Cells* **2008**, *92*, 814−818.
(37) Korkut, S.; Roy-Mayhew, J. D.; Dabbs, D. M.; Milius, D. L.; Aksay, I. A. *ACS Nano* **2011**, *5*, 5214−5222.
(38) Brunauer, S.; Emmett, P. H.; Teller, E. *J. Am. Chem. Soc.* **1938**, *60*, 309−319.